

Alternative operational strategies for wind turbines in cold climates

Stoyanov, D. & Nixon, J.

Author post-print (accepted) deposited by Coventry University's Repository

Original citation & hyperlink:

Stoyanov, D & Nixon, J 2020, 'Alternative operational strategies for wind turbines in cold climates' *Renewable Energy*, vol. 145, pp. 2694-2706.

<https://dx.doi.org/10.1016/j.renene.2019.08.023>

DOI 10.1016/j.renene.2019.08.023

ISSN 0960-1481

ESSN 1879-0682

Publisher: Elsevier

NOTICE: this is the author's version of a work that was accepted for publication in *Renewable Energy*. Changes resulting from the publishing process, such as peer review, editing, corrections, structural formatting, and other quality control mechanisms may not be reflected in this document. Changes may have been made to this work since it was submitted for publication. A definitive version was subsequently published in *Renewable Energy*, 145, (2020)

DOI: 10.1016/j.renene.2019.08.023

© 2019, Elsevier. Licensed under the Creative Commons Attribution-NonCommercial-NoDerivatives 4.0 International

<http://creativecommons.org/licenses/by-nc-nd/4.0/>

Copyright © and Moral Rights are retained by the author(s) and/ or other copyright owners. A copy can be downloaded for personal non-commercial research or study, without prior permission or charge. This item cannot be reproduced or quoted extensively from without first obtaining permission in writing from the copyright holder(s). The content must not be changed in any way or sold commercially in any format or medium without the formal permission of the copyright holders.

This document is the author's post-print version, incorporating any revisions agreed during the peer-review process. Some differences between the published version and this version may remain and you are advised to consult the published version if you wish to cite from it.

Alternative Operational Strategies for Wind Turbines in Cold Climates

D. B. Stoyanov and J. D. Nixon*

Faculty of Engineering, Environment and Computing

Coventry University, 1 Gulson Road, Coventry, CV1 2JH, UK

*corresponding author, E-mail: jonathan.nixon@coventry.ac.uk; Tel: 024 7765 3151

Abstract

Around a quarter of the global wind energy capacity is operating in cold climates, where ice accretion can damage wind turbines, cause safety concerns and reduce power output. In this paper, alternative operational strategies to reduce ice build-up and increase power output are studied. The alternative strategies are achieved by making tip-speed ratio (TSR) modifications both during and after an icing event. To compare different TSR strategies, the concept of an energy payback time is outlined, which is used to determine when an alternative strategy outperforms a turbine's normal design strategy. The method is demonstrated using the NREL 5 MW reference wind turbine for twelve different icing conditions, encompassing different temperatures, wind speeds, droplet diameters and liquid water contents. The results indicate that for short and severe icing events, an alternative TSR strategy will start producing more energy than a conventional design strategy within 0.5-2.5 hours after icing and decrease ice accumulation by approximately 25-30% per blade. The method presented in this study will enable more effective operational control strategies to be deployed for minimising ice-induced power losses and ice accretion at wind farms located in cold climates.

Key Words: Ice accretion; Wind Power; Wind Energy; Tip-Speed Ratio (TSR); Aerodynamics; Icing events.

30 Nomenclature

31 Variables

32	a	Axial induction factor	(-)
33	a'	Tangential induction factor	(-)
34	c	Aerofoil chord length	(m)
35	C _p	Power coefficient	(-)
36	E	Energy	(MWh)
37	LWC	Liquid water content	(kg.m ⁻³)
38	M	Mass	(kg)
39	MVD	Median volume diameter	(m)
40	P _w	Wind power	(W)
41	r	Blade radius	(m)
42	T	Temperature	(°C)
43	t	Time	(h)
44	TSR	Tip-speed ratio	(-)
45	V	Wind speed	(m.s ⁻¹)

47 Greek

48	ρ	Air density	(kg.m ⁻³)
49	ω	Rotor Rotational Speed	(rad.s ⁻¹)

51 Subscripts

52	AI	After icing
53	DI	During icing
54	EPB	Energy payback
55	M	Modified operational strategy
56	R	Reference operational strategy
57	rel	Relative to the blade

59 Acronyms

60	AoA	Angle of attack
61	BEMT	Blade element momentum theory
62	CC	Cold climate
63	NREL	National Renewable Energy Laboratory

64

1 Introduction

By the end of 2017, the global wind energy capacity was approximately 540 GW [1]. Nearly a quarter of the installed capacity is expected to be at risk of icing due to cold climate (CC) conditions [2]. Locations classified as CCs are typically characterised by a high wind resource availability [3]. However, in such conditions, the efficiency of wind turbines can be severely compromised by the prevalence of icing, reducing power output [4-7], causing structural damage and decreasing wind turbines' life span [7,8]. Ice induced power losses can be extremely variable depending on location, wind turbine scale and weather conditions [7,9]. This can make it difficult deciding where to locate a wind turbine and how to operate it in CCs. As a result, annual losses reported for wind turbines in CCs can often reach 20% [5].

Most commercial wind turbine blades are designed as lift generating devices and ice build-up on the aerofoils typically decreases lift and increases drag. This reduction in aerodynamic efficiency is generally well known from previous research on aircraft icing [10-13], and many studies are now focusing on the implications for the wind energy industry.

A significant amount of research has been carried out on how ice forms on wind turbines [11,14], impacts power output [5,13,15] and affects structural robustness [14,16]. Thus, it has been established how much more severe icing is for longer icing events, larger water droplet sizes and liquid water contents, smaller chord lengths and higher wind speeds. In addition, it is known that ice thickness increases approximately linearly from the root to the tip of the blade when considering a 2D analysis and not accounting for ice shedding [16]. Although more research is needed to substantiate these results and classify them in a useful database, there is a particular need to utilise these findings and search for more efficient approaches to operate wind turbines in icing conditions [17]. An efficient wind turbine operational strategy can minimise annual power losses, prevent structural damage and reduce wind turbine downtime. However, there are only a limited number of studies that have looked at improving wind turbines operational efficiency in icing conditions by applying different tip-speed ratio (TSR) strategies.

Homola et al. [18] and Zanon et al. [19] investigated the operation of the National Renewable Energy Laboratory (NREL) 5 MW reference wind turbine in icing conditions. Both studies analysed the performance of the wind turbine considering the torque-speed curve and the torque-speed controller. Homola et al. [18] simulated the iced performance of the wind turbine after a one-hour long icing event, operating the wind turbine either by adapting the torque-speed controller to the iced-torques-speed curve or by modifying the controller to maintain the TSR at its design value. When examining the wind turbine power curve for the iced blade and bypassing the controller, a 10% higher achievable power output for velocities between 7 and 13 ms^{-1} was reported, while slightly higher power losses were seen for wind speeds of 3 and 6 ms^{-1} . As

97 the study focused on a single icing condition, the authors highlighted the need for further analysis of more
98 severe icing cases. Zanon et al [19] analysed the wind turbine's performance during an active icing period
99 and showed the influence of three different TSR operational strategies on the ice-induced power losses.
100 The study showed how the ice-induced losses can be mitigated by reducing the TSR during an icing event.
101 However, a reduction in the ice-induced power losses, does not necessarily mean that overall energy
102 generation would be increased.

103 By reducing the TSR during an icing event to minimise ice build-up, the reference TSR could be restored
104 once an icing event ends to improve performance [20]. However, the reference TSR may no longer be the
105 best post-icing event operational strategy due to ice remaining on the blades and changes in aerodynamic
106 behaviour. To determine if gains in energy generation can actually be achieved, a turbine's performance
107 needs to be analysed throughout and immediately after an icing event. This approach could also be used to
108 implement an operational strategy to both reduce ice build-up during an event and maximise post-icing
109 event power output. Moreover, a method for comparing and evaluating different TSR operational strategies
110 is needed and the performance analysis needs to be applied for a wide range of different icing conditions.

111 This study aims to establish a method for evaluating different operational strategies based on tip-speed
112 ratio modifications made both during and after an icing event. This is achieved by introducing the concept
113 of an energy payback time, which is based on the time taken for an alternative TSR strategy to start
114 producing more energy than the reference operational regime after the end of an icing event. By
115 considering a wide range of different icing events, wind speeds and ambient temperatures, the study sets
116 out to determine when an alternative operational strategy should be used to reduce ice build-up during an
117 icing event and increase energy yield once an event ends.

118 Section 2 specifies the methods used to carry out the study including definition of the icing model, iced
119 blade aerodynamic performance, icing events considered and energy payback parameter based on ice
120 accretion and modified power coefficients. The results and suggestions for further work are discussed in
121 Section 3, and the paper's conclusions are provided in Section 4.

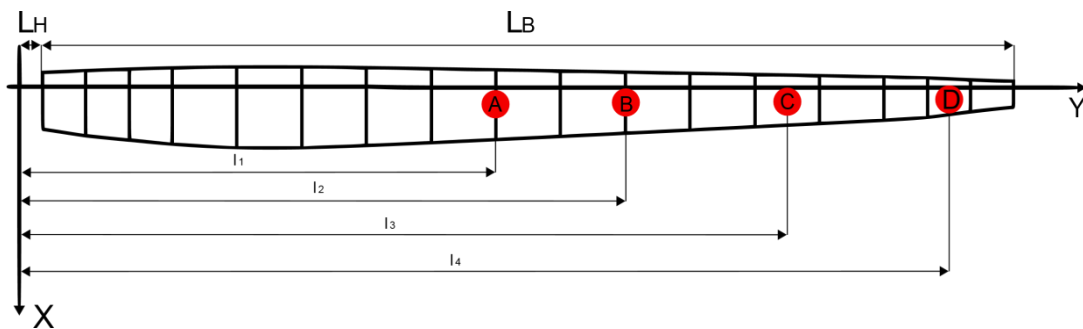
122 2 Method

123 In this study, three typical icing events are considered to evaluate a number of different operational
124 strategies based on varying tip-speed ratios. Furthermore, each event is tested for three different wind
125 speeds (5, 7 and 10ms⁻¹) and two ambient temperatures (-5 and -10°C). To simulate ice formation during
126 these events, LewINT[®] ice accretion software is used as it is the most widely established tool for generating
127 2D ice shapes on aerofoils and it has been validated extensively for aircraft icing [21,22]. LewINT[®] is based
128 on source and dipole singularities superposition panel method to obtain flow velocities, which are used to

129 calculate droplet trajectories, aerofoil surface water fluxes and energy balance for the ice shape
 130 calculations. Qblade is utilised for the power performance analysis [23]; it incorporates Blade Element
 131 Momentum Theory (BEMT) for power analysis and XFOil [24] for the aerodynamic analysis, which utilises
 132 vortex and source singularities panel method together with integral boundary layer method. Both methods
 133 have been widely used and allow for relatively low computationally intensive simulations to be carried out.
 134 The wind turbine chosen for the study is the NREL 5 MW reference wind turbine [25], as it is commonly
 135 used in the literature for this type of study.

136 2.1 Ice Accretion Modelling

137 To reduce the number of required simulations, four sections of the wind turbine blade are modelled to
 138 determine the ice accumulation along its length during the icing events. Figure 1 shows the sections, which
 139 are considered between the half-span and the full span of the blade: sections A, B, C and D. The distances
 140 from the blades centre of rotation are as follows: l_1 is $0.52r$, l_2 is $0.65r$, l_3 is $0.80r$ and l_4 is $0.94r$ with r being
 141 the local blade radius. The hub radius, L_H , and blade length, L_B , are 1.5 m and 61.5 m, respectively. The
 142 aerofoils corresponding to the chosen blade sections are DU 91W225 for Section A, DU 93W21LM for
 143 Section B and NACA 64618 for sections C and D. As minimal icing occurs on the inner-blade sections, they
 144 have not been considered during the ice accretion simulations [19].



145 Figure 1: Discretised NREL 5 MW blade and the selected 2D sections for ice accretion analysis.

146 The ice formation analysis has been conducted using the 2D aerofoil sections at each of the four
 147 discretised locations. Symmetrical ice deposition across the turbine's three blades is assumed with uniform
 148 ice geometry for each iced section. The relative speed to the blade sections is calculated using classic
 149 BEMT theory, Eq. 1, where V_{rel} is the relative speed to the blade, V is the wind speed, ω is the rotational
 150 speed of the rotor, r is the local blade section radius, and a and a' are the axial and tangential induction
 151 factors, respectively. The ice mass is estimated by using the predefined ice density of $917 \text{ kg}\cdot\text{m}^{-3}$ in LewINT
 152 [21].

$$V_{rel} = \sqrt{(V(1 - a))^2 + (\omega r(1 + a'))^2} \quad (1)$$

Using low computationally intensive tools allows for the simulation of a variety of icing events in a relatively short time. However, this does reduce the accuracy of the aerodynamic analyses. XFOil is a two-dimensional tool, which incorporates the integral boundary layer equations in the viscous boundary layer and potential flow equations in the outer inviscid region; the two regions are coupled using a viscous-inviscid interaction scheme. Due to the use of XFOil and 2D analysis, increased uncertainty is expected for cases where separated flow occurs, e.g. for high angles of attack (AoA) or highly irregular ice shapes.

2.1.1 Icing Events Definition

To study wind turbine performance during different in-cloud icing events, encompassing rime, mixed and glaze icing conditions, a number of icing events are defined based on published experimental [26] and field data [27,28]. The different ice modelling parameters that need to be considered include liquid water content (LWC), median volume diameter (MVD) and icing event duration (t_{Event}). Each parameter can vary widely for different locations and especially for different orographic features. In-cloud icing conditions are mostly pronounced in hilly and mountainous terrains, where wind turbine blades can reach the low-level cloud base (300-1200m) during winter months [28]. A typical MVD for in-cloud icing is $20 \times 10^{-6} \text{m}$ [26], but it can range from 10 - $35 \times 10^{-6} \text{m}$ [28]. The LWC is normally $3 \times 10^{-4} \text{kg.m}^{-3}$ [26], and ranges from 0.4 - $3.5 \times 10^{-4} \text{kg.m}^{-3}$ [28,29]. Ice events tend to be shorter for larger liquid water contents and size droplets [29,30] and typical durations range from 20 min to 48 hours, while in some cases up to several weeks [29].

During an icing event, wind speed (V) and ambient temperature (T) significantly influence the type of ice being accreted. Thus, three icing events (defining LWC, MVD and duration) are chosen along with different wind speeds and ambient temperatures that are most likely to occur. Table 1 shows icing event A (LWC of $5 \times 10^{-4} \text{kg.m}^{-3}$ and MVD of $25 \times 10^{-6} \text{m}$), B (LWC of $3 \times 10^{-4} \text{kg.m}^{-3}$ and MVD of $20 \times 10^{-6} \text{m}$) and C (LWC of $0.4 \times 10^{-4} \text{kg.m}^{-3}$ and MVD of $12 \times 10^{-6} \text{m}$), which are modelled at different temperatures (-5°C and -10°C) and wind speeds (5 , 7 and 10m.s^{-1}) giving a total of 12 different icing cases. Event A represents the harshest conditions, which typically occur for a relatively short duration, and events B and C are mild and light conditions respectively.

Table 1: Definition of icing events A, B and C, at different wind speeds (V) and temperature (T).

Event, V, T	LWC (kg.m^{-3})	MVD (μm)	Duration, t_{Event} (s)	(V (m.s^{-1}))	T ($^\circ\text{C}$)
A1010	5	25	1	10	-10
A105	5	25	1	10	-5
A710	5	25	1	7	-10
A75	5	25	1	7	-5

A510	5	25	1	5	-10
A55	5	25	1	5	-5
B1010	3	20	4	10	-10
B710	3	20	4	7	-10
B75	3	20	4	7	-5
B510	3	20	4	5	-10
C105	0.4	12	4	10	-5
C1010	0.4	12	4	10	-10

178

179 2.2 Operational Strategy

180 The control parameter used in this study is TSR and its setting during (TSR_{Di}) and after (TSR_{Ai}) an icing
181 event. The TSR changes can be implemented by either prescribing constant TSR during the event or by
182 adapting the torque-speed controller to the iced torque-speed curve [19]. In this work, steady state
183 simulation of the icing process and the aerodynamic effects is considered, similarly to previous research
184 [16,18]. It is assumed that the TSR during icing will remain constant as the icing durations in the current
185 study are short enough and the natural degradation of the TSR will be small [19]. The possible TSR values
186 that can be set are chosen according to the rated (maximum) rotational speed (seldom synchronous and
187 asynchronous generators are operated above their rated speed) and the minimum rotational speed,
188 required for energy generation. Considering the NREL 5 MW generator [25] with a minimum RPM of 670
189 and maximum of 1173.7RPM, the possible TSR limits (TSR_{Min} and TSR_{Max}) for operation can be determined
190 (see Figure 2). The reference TSR design strategy is shown by TSR_R and Figure 2b shows how the
191 coefficient of power (C_p) varies at different TSR settings for a non-iced blade. During an icing event, it is
192 assumed that the controller will allow intentional energy yield reduction by reducing the tip-speed ratio,
193 thereby reducing ice accretion and enabling an improved C_p to be obtained once the event finishes [14].

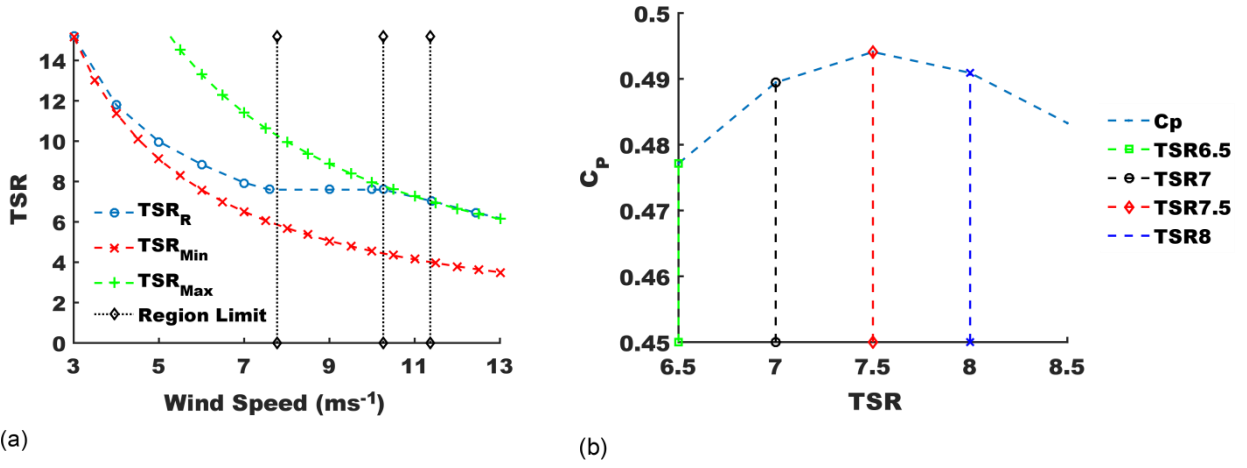


Figure 2a-b: NREL 5 MW reference wind turbine TSR operational limits defined by the limiting rotational speeds of the electrical generator (a) and how the power coefficient varies at different TSR (b).

2.3 Energy payback time

The energy payback time, t_{EPB} , defines how long it will take an alternative modified operational strategy (TSR_M) to start producing more power than the turbine's reference strategy (TSR_R). Figure 3a depicts the reduction of the instantaneous power output during an icing event by operating with an alternative TSR_{DI} , and the potential for improving performance at the end of an icing event by increasing the TSR_{AI} due to less accreted ice and better power characteristics. To compare a modified and reference operational strategy, the cumulative energy harvested during and after an event needs to be determined (see Figure 3b). The cumulative energy produced during icing, E_{DI} , is found from the available power in the wind, P_w , and the power coefficient, C_p , which varies throughout the duration of the icing event and depends on the chosen TSR (Eq. 3). P_w is defined by the air density, ρ , wind speed, V , and wind turbine blade radius, r (Eq. 2).

$$P_w = 0.5\rho V^3 \pi r^2 \quad (2)$$

$$E_{DI} = \int P_w C_p(TSR, t) dt \quad (3)$$

The assumption is made that for a short period (<48 hours) after the end of an icing event, no significant ice melting or shedding will occur. This assumption is based on the consideration of winter anticyclone weather conditions with low temperatures and wind speeds that could span up to a week or more after an in-cloud icing event [31]. The coefficient of power will remain constant, if the assumption is made that the iced blade geometry will not change significantly soon after the end of an icing event. Thus, the cumulative net energy output will be linear as C_p defines the rate of energy yield. The energy produced after an icing event by the reference ($E_{AI,R}$) and modified ($E_{AR,M}$) operational strategies can be represented by equations Eq.4 and Eq. 5, respectively. The rate of cumulative energy after the icing event is calculated in addition to the total

212 energy produced during the icing event (E_{DI}); $E_{DI,R}$ and $E_{DI,M}$ are respectively the cumulative energy
 213 produced during the icing event for the reference and modified operational strategies. The time taken for
 214 the modified strategy to payback the lost energy during icing is determined when $E_{AI,R}$ equals $E_{AI,M}$; making
 215 t_{EPB} the subject of the equation results in Eq. 6. When estimating t_{EPB} , it should be noted that the results are
 216 only an indication for the potential effectiveness of an alternative strategy and extremely large values would
 217 suggest that alternative solutions to the TSR strategy should be considered and melting and shedding
 218 would need to be taken into account to obtain more accurate t_{EPB} values.

$$E_{AI,R} = P_W C_{p(TSR_{AI,R})} t_{EPB} + E_{DI,R} \quad (4)$$

$$E_{AI,M} = P_W C_{p(TSR_{AI,M})} t_{EPB} + E_{DI,M} \quad (5)$$

$$t_{EPB} = (E_{DI,R} - E_{DI,M}) / [P_W (C_{p(TSR_{AI,M})} - C_{p(TSR_{AI,R})})] \quad (6)$$

219

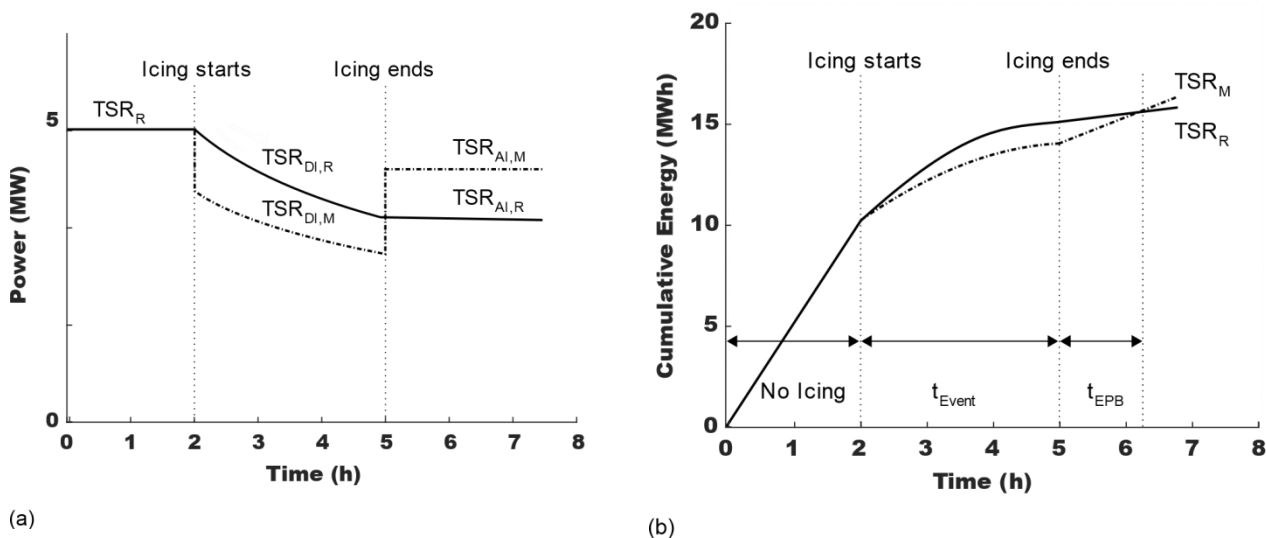


Figure 3a-b: Power output (a) and cumulative energy (b) during and after an icing event for a wind turbine operating with a reference (TSR_R) or modified (TSR_M) tip-speed ratio strategy.

220

221 3 Results and Discussion

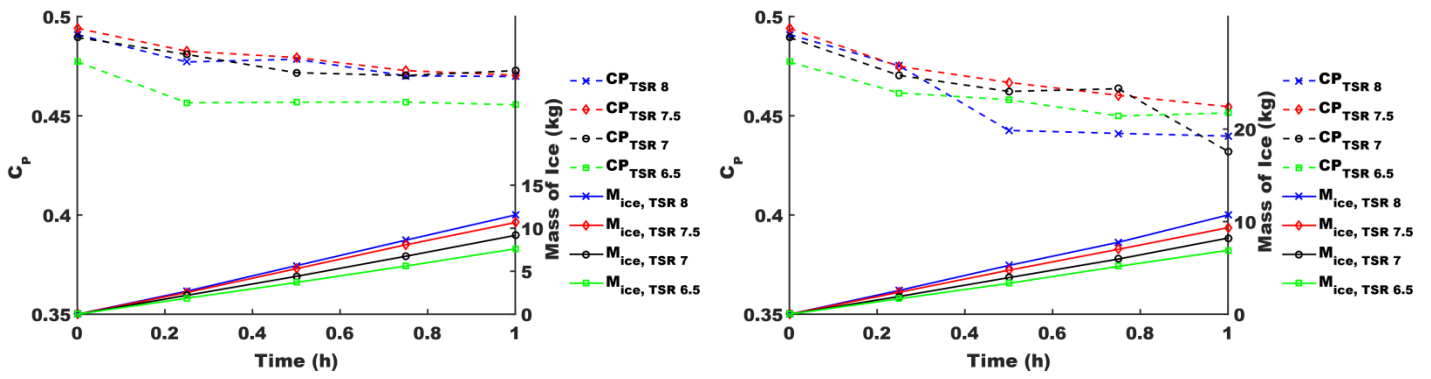
222 3.1 Results

223 For each icing condition, C_p degradation, ice accumulation, final ice shapes for section D, ice induced
224 power losses, rotor power characteristics, $C_p(t)$, at the end of the event and energy payback times are
225 presented in this section. In total 1176 ice shapes were generated for all icing events, with 180 ice shapes
226 per timestep being analysed. Ice mass and C_p degradation were estimated considering all 1176 ice
227 shapes, while the power characteristics and t_{EPB} were analysed investigating the ice shapes at the end of
228 the icing events. All final ice shapes at the modelled blade locations are provided in the Supplementary
229 Online Appendix, while in this section only the most heavily iced blade location has been presented
230 (section D, see Figure 1). Ice-induced power losses and total harvested energy before and after an event,
231 considering all modelled blade sections, were the main parameters used for the comparison of alternative
232 TSR_{DI} and TSR_{AI} strategies. Ice mass for each strategy on a single blade is shown, but aeroelastic effects
233 and component loads are beyond the scope of this work as for similar icing conditions it has been shown
234 that the effects on the structural loading from additional ice mass are minimal [14,16].

235 3.1.1 Event A

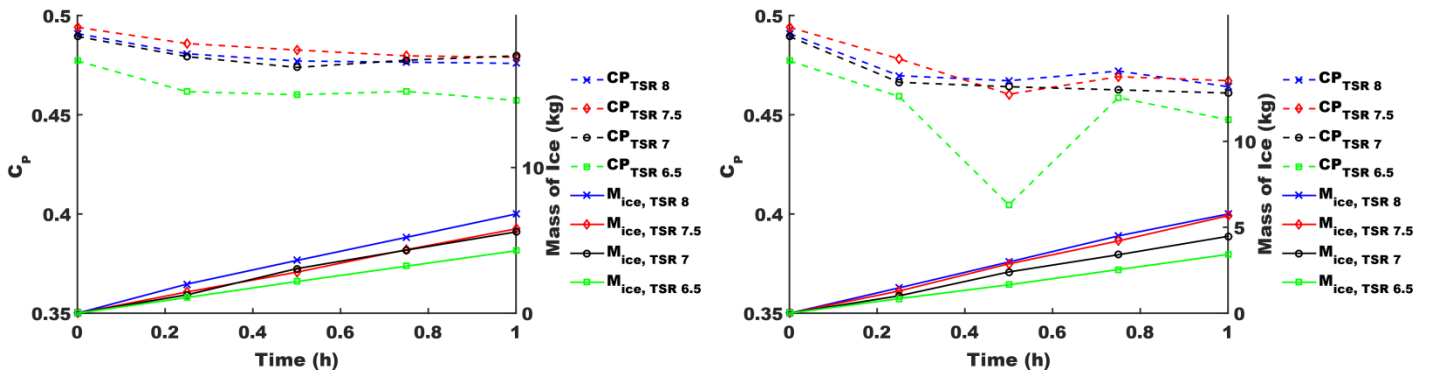
236 Event A has been simulated for wind speeds of 10, 7 and 5 ms^{-1} and ambient temperatures of -10 and -
237 5°C, resulting in 6 cases – A1010; A105; A710; A75; A510 and A55. E.g. A1010 represents the LWC, MVD
238 and duration defined by Event A in Table 1, occurring with a wind speed of 10 ms^{-1} and an ambient
239 temperature of -10°C.

240 The deterioration of C_p for the whole simulated wind turbine rotor and the ice mass accumulation for each
241 blade for all cases of Event A are presented on Figure 4a-f. Alternative viable operational TSRs of 6.5 to 8
242 for wind speeds of 10 and 7 ms^{-1} (Figure 4a-d) and TSRs of 9 to 10 for wind speed of 5 ms^{-1} (Figure 4e-f)
243 are shown. TSR values greater than TSR_R for a wind speed of 5 ms^{-1} are not considered for the analysis,
244 as it would result in a high V_{rel} and ice build-up (see Figure 2a). As the ice accumulation rate is a function of
245 the blade's relative velocity [9,14], less ice deposition is apparent when the ambient temperature increases
246 and both the wind speed and the TSR decrease (see Figure 4). The highest amount of accreted ice per
247 blade is 11.5 kg for case A1010; the least is 4 kg for case A55. As the type of ice being formed can change
248 from one type to another for the same icing case (rime to glaze) and it can vary along the blade of utility
249 scale wind turbines, the power convergence efficiency does not degrade linearly. Depending on the type of
250 accreted ice and the disturbance of the flow over the blade, the C_p decreases either gradually (A1010,
251 A710 and A510) or more sharply (A105, A75 and A55).



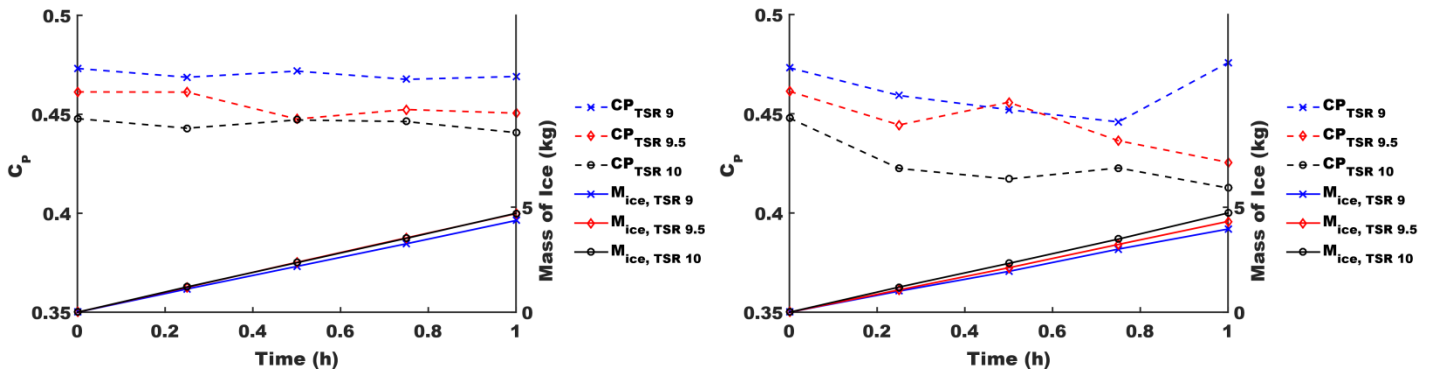
(a) Case A1010

(b) Case A105



(c) Case A710

(d) Case A75



(e) Case A510

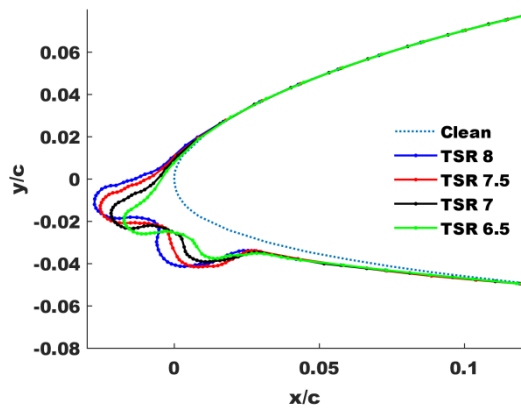
(f) Case A55

Figure 4a-f: Wind turbine power coefficient degradation and total ice mass accumulation per blade during events A1010 (a), A105 (b), A710 (c), A75 (d), A510 (e) and A55 (f).

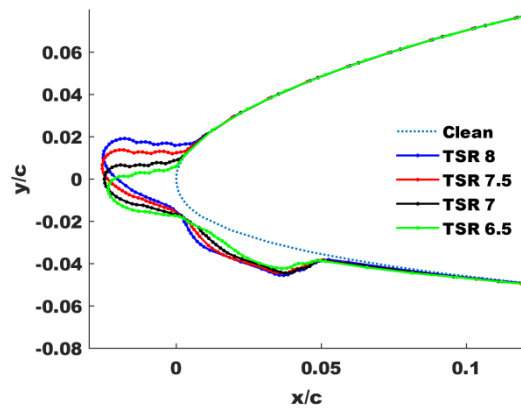
252 Final ice shapes for blade Section D (see Figure 1) are displayed on Figure 5a-f. The ice shapes for A105,
 253 A75 and A55 are typical for glaze icing conditions. They are characterised by having a less conformal
 254 geometry to the aerofoil contour and the presence of one or two horns [26]. The shapes for A510 are
 255 typical for rime ice cases as they are more conformal to the aerofoil geometry. Higher energy losses are

256 expected for glaze and mixed icing conditions [14]. As these shapes produce more complex wall bounded
257 flow, the aerodynamic uncertainties from the simulations tend to be higher, which is represented by the
258 greater C_p fluctuations obtained for events A105, A75 and A55 (Figure 4b, d and f). Higher fidelity analyses
259 over a smaller range of time steps are needed to further investigate these specific flow features and
260 fluctuations in the results. For cases A1010, A710 (Figure 5a and c) the ice shapes are representative for
261 mix-type icing, being conformal to the aerofoil contour at first (rime) and subsequently forming horn-like
262 protrusions. The flatter C_p profiles for Events A1010, A710 and A510 (Figure 4a, c and e) are attributed to
263 ice forming normal to the leading edge or on the pressure side of the aerofoil causing less aerodynamic
264 disturbance [10] (see Figure 5a,c and e).

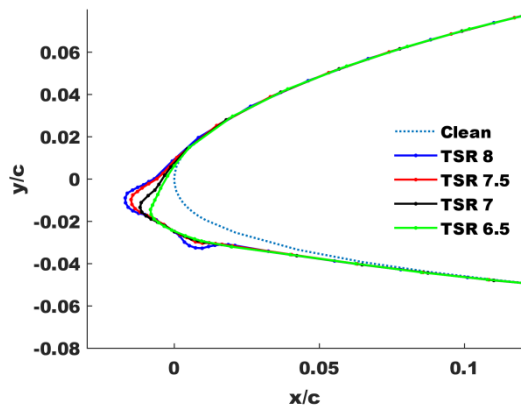
265



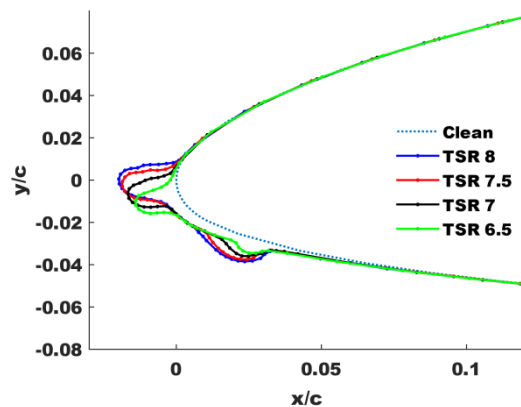
(a) Case A1010



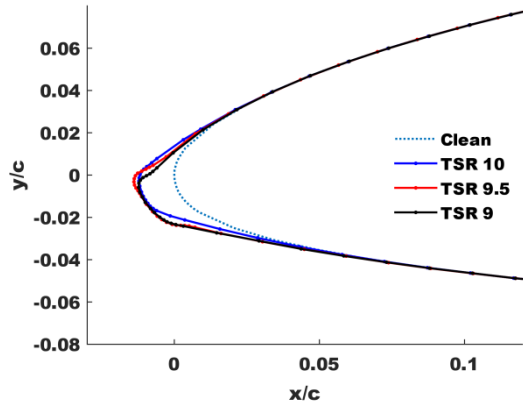
(b) Case A105



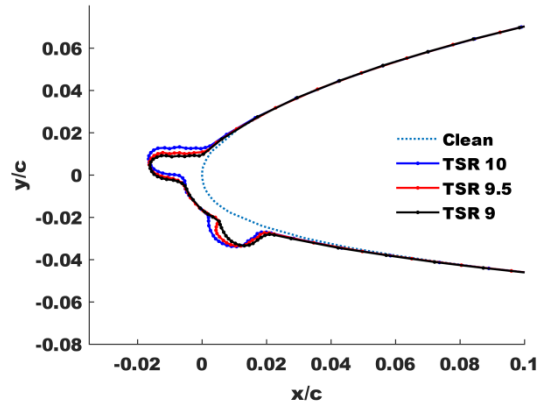
(c) Case A710



(d) Case A75



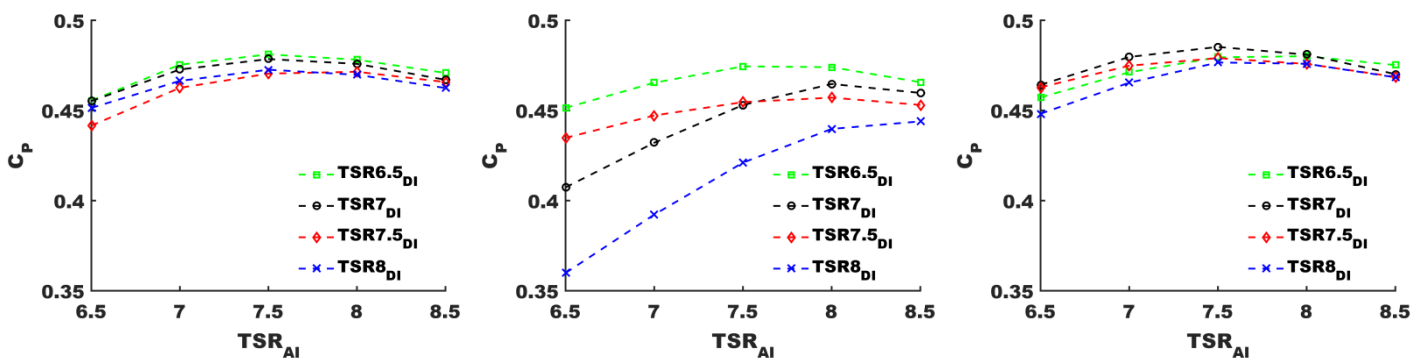
(e) Case A510



(f) Case A55

Figure 5a-f: Ice shapes on Section D for event cases A1010 (a), A105 (b), A710 (c), A75(d), A510 (e) and A55 (f).

Figure 6a-f reveals how setting different TSR values can be used to minimise power losses during icing and maximise performance after an icing event ends. Specifically, the results show the power coefficients of the iced wind turbine at the end of the icing events for different TSR_{DI} values, and subsequent power coefficients that can be obtained with a new TSR_{AI} value. As expected, the minimum TSR_{DI} typically provides the best possible post-icing performance, due to less ice having deposited on the rotor blades. The exception is case A710, where the differences between alternative TSRs are negligible due to the relatively small accumulation of ice. For example, Figure 6d shows that the turbine could be slowed down to a TSR_{DI} of 6.5 with TSR_{AI} increased to 8 to achieve a power coefficient of over 0.475. These results also highlight how significant the degradation of C_p can be for the TSR_R value of 7.5 (Figure 6a-d) and that restoring TSR_{AI} to 7.5 would improve the power performance after icing in events A1010 and A105. To maximise the power output and minimise the icing losses for a wind speed of 5 ms^{-1} , both TSR_{DI} and TSR_{AI} should be 9 as it provides higher C_p at lower rotor rotational speeds, but the viability of this depends on the coupled electrical generator.



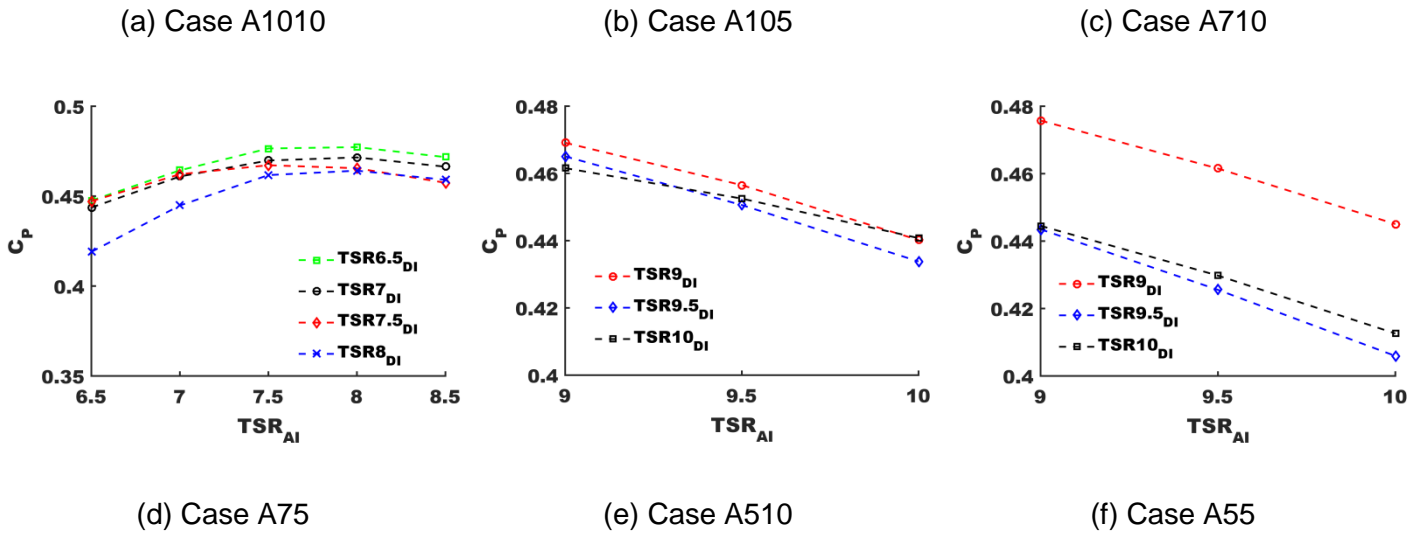
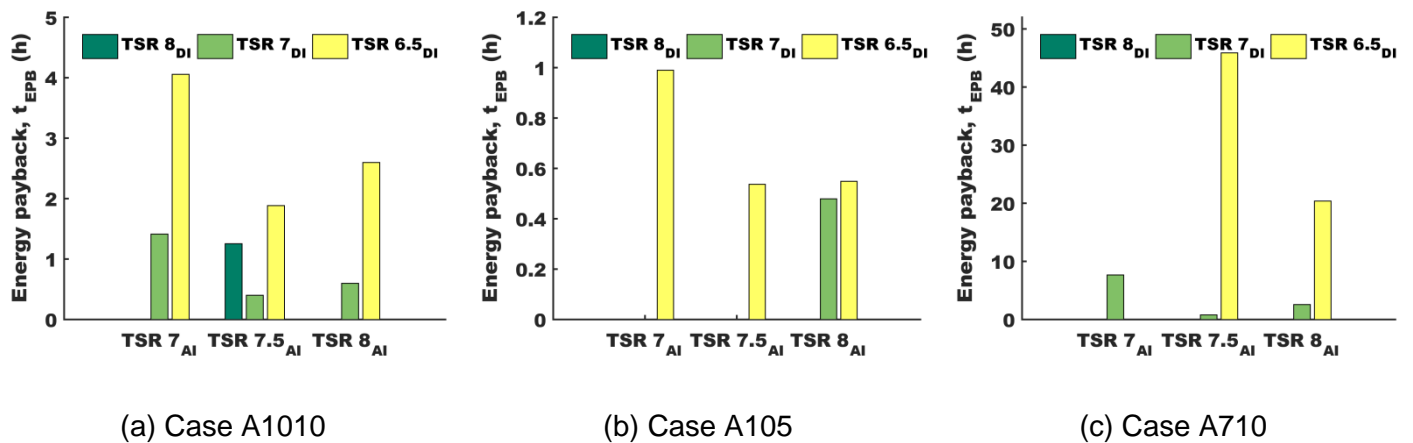
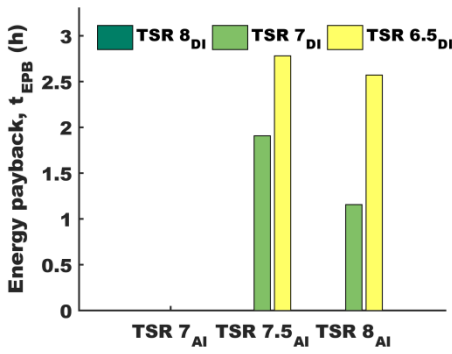


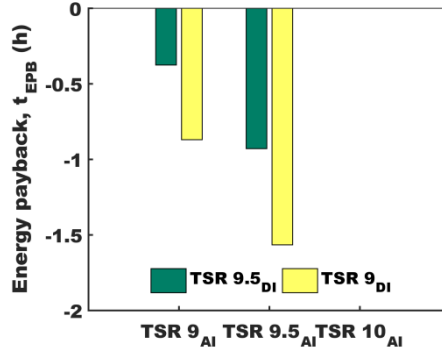
Figure 6a-f: Power characteristics of modified tip-speed ratio values after icing events A1010 (a), A105 (b), A710 (c), A75(d), A510 (e) and A55 (f).

279 The time it would take to replace the lost energy for reducing the TSR during the icing event, t_{EPB} , is shown
 280 for Event A on Figure 7a-f. It is noticeable how sensitive t_{EPB} is to variations in wind speed, ambient
 281 temperature and TSR operational regime. For Event A at wind speeds of 7 and 10ms⁻¹ (Figure 7a-f), the
 282 most beneficial TSR_{DI} is 7 with TSR_{AI} set to either 7.5 or 8, which provides energy payback times of around
 283 0.5-2.5 hours. Interestingly, if the TSR_{AI} was to be restored to the turbines reference speed (TSR_R) of 7.5
 284 after event A105, the only TSR_{DI} and resulting characteristics that could replace the lost energy would be
 285 $TSR_{6.5_{DI}}$. For event cases A510 and A55, C_p is improved for a reduced TSR value both during and after
 286 the icing events, so there is no energy payback, and this suggests that the reference design strategy could
 287 be improved for non-icing conditions. As a result, the energy payback time appears negative in Figure 7e
 288 and 7f.

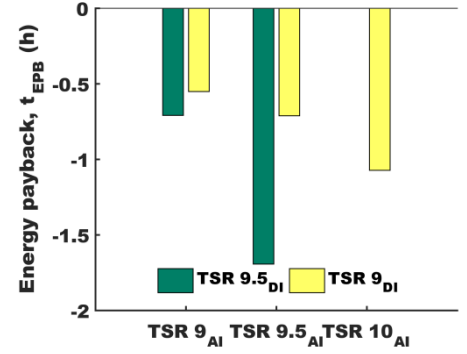




(d) Case A75



(e) Case A510



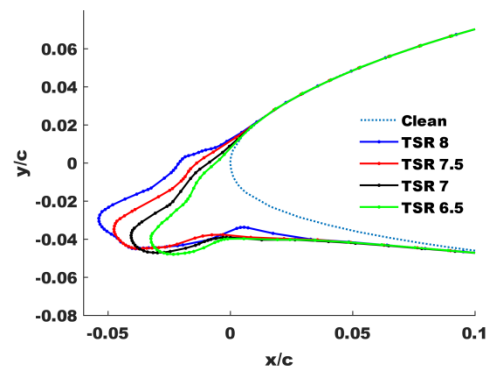
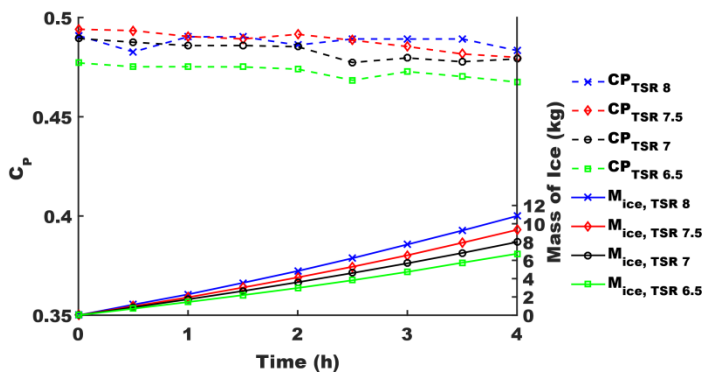
(f) Case A55

Figure 7a-f: Energy payback time for different tip-speed ratio after icing (TSR_{AI}) values for events A1010 (a), A105 (b), A710 (c), A75(d), A510 (e) and A55 (f).

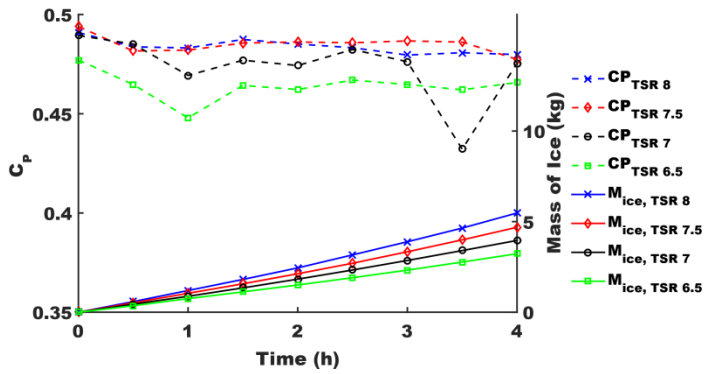
289

290 3.1.2 Event B

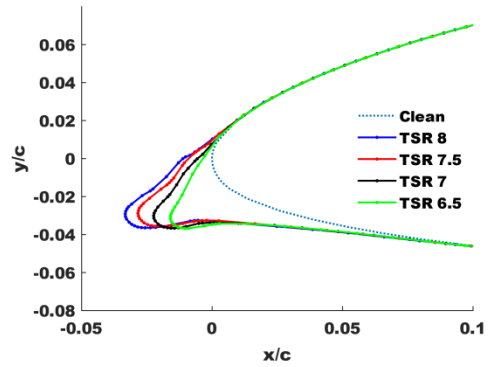
291 In comparison to Event A, the C_p degradation for all Event B cases is more gradual due to a reduced ice accretion rate and more conformal ice shapes to the blade geometry (see Figure 8a-h). The sudden C_p
 292 drop for B710 and B75 during the first hour of icing is an interesting observation and can be attributed to
 293 the way the ice shapes form during the event. As the ice shapes are representative for rime and mixed-type
 294 icing, they are conformal to the clean geometry until the thermodynamic equilibrium changes on the air-ice
 295 boundary. It is apparent that before the thermodynamic equilibrium changes, the rime shapes during the
 296 first hour of icing are characterised by greater leading edge curvature slopes than the ice shapes at the end
 297 of the event. Due to the nature of the panel method algorithm, greater curvature slopes lead to reduced
 298 accuracy of the analysis. The aerodynamic uncertainties for B710 and B510 indicate ice shapes with
 299 increased curvature slopes near the leading edge region occurring during the 3rd hour of icing. This
 300 highlights the need for a greater fidelity aerodynamic analysis of such conditions.
 301



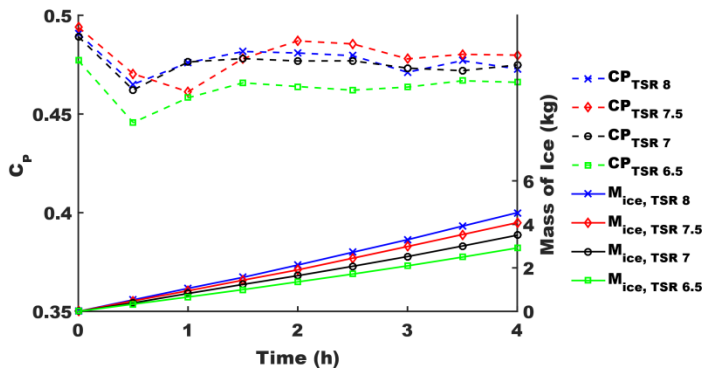
(a) case B1010



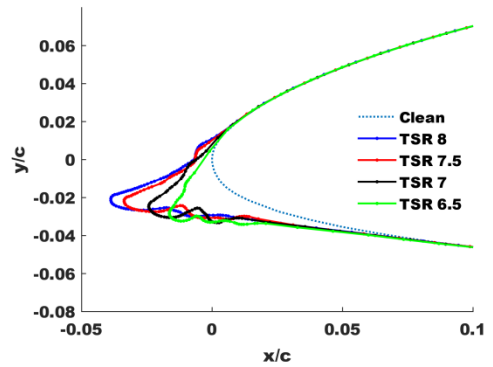
(b) case B1010



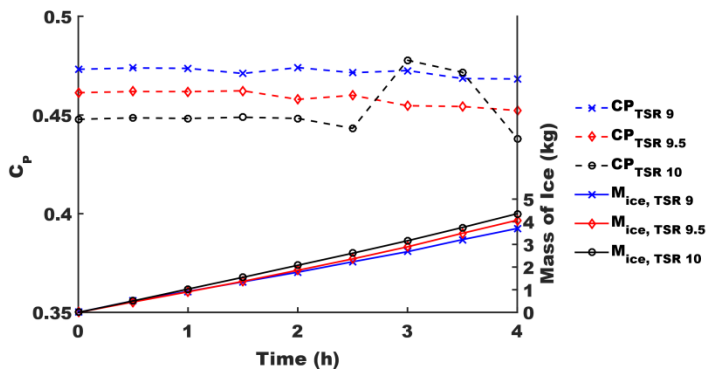
(c) Case B710



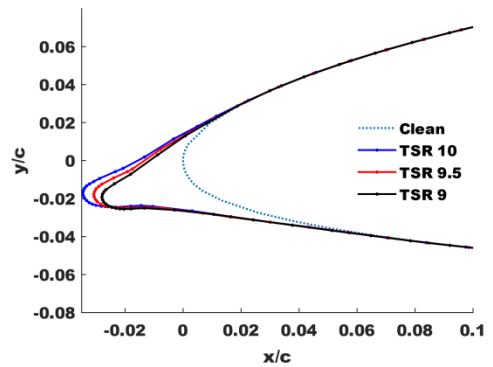
(d) Case B710



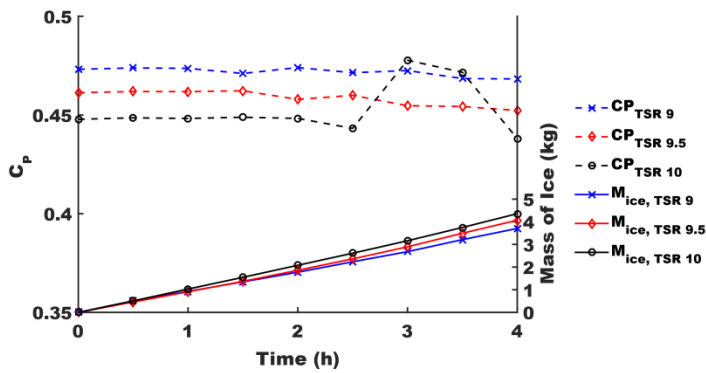
(e) Case B75



(f) Case B75



(g) Case B510



(h) Case B510

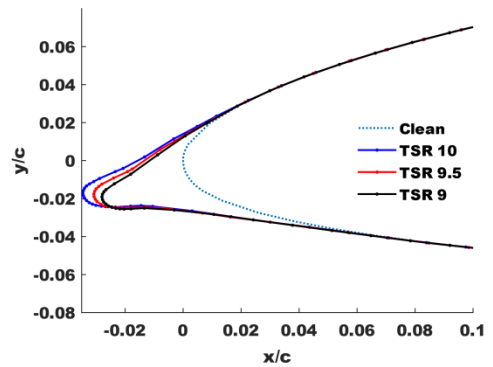


Figure 8a-h: Wind turbine C_p deterioration and ice accumulation per blade during events B1010 (a), B710 (c), B75 (e), B510 (g) and ice shapes on section D at the end of events B1010 (b), B710 (d), B75 (f), B510 (h).

302

303

304

305

306

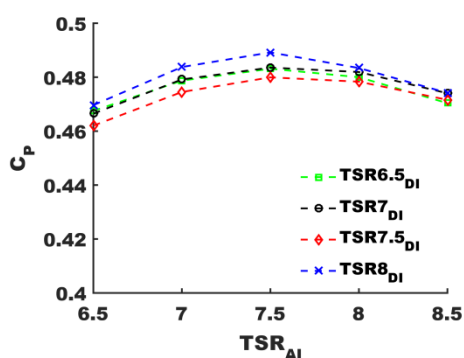
307

308

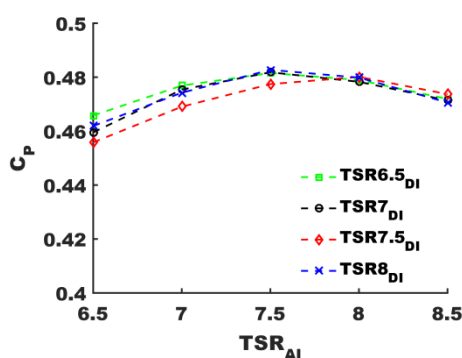
309

310

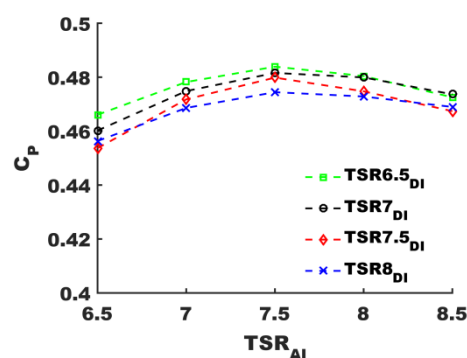
The TSR_{AI} power characteristics for shapes produced during Event B cases are not particularly sensitive to changes in TSR_{DI} . Figure 9a-d shows that only minimal performance improvements can be achieved after icing by slowing the rotor down during the icing event. Unlike for Event A, only event B75 results in a TSR_{DI} of 6.5 being the preferred option for post-icing operation. Similarly, the minimum TSR_{DI} for event B510 provides the most favourable power characteristics after icing. The maximum TSR_{DI} of 8 indicated as the best option for B1010 is likely due to the discrepancies of the aerodynamic analysis and the negligible differences in the aerodynamic performance of the produced ice shapes under these conditions and TSR_{DI} values.



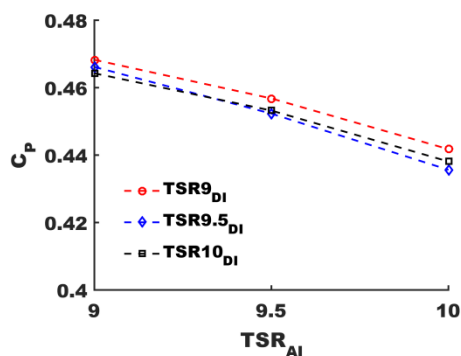
(a) case B1010



(b) case B710



(c) case B75



(d) case B510

Figure 9a-d: Power characteristics of modified tip-speed ratio values after icing events B1010 (a), B710 (b), B75(c) and B510 (d)

311

312

313

The minimal performance improvement observed from reducing the TSR_{DI} indicates that the energy payback time will be long or unachievable. Reducing to a TSR_{DI} of 7 and increasing to a TSR_{AI} of 7.5 would have a long energy recovery time of 6h for B1010, 11.5h for B710 and 8.5h for B75. For $TSR_{6.5DI}$ this

314 would increase to 19.5h, 21.3h and 16h for events B1010, B710 and B75, respectively. For some TSRs,
 315 t_{EPB} can reach extreme values (48-200h), which indicates that alternative ice mitigation approach should be
 316 considered or, if the power losses are too high, complete shutdown would be advisable. With a TSR_{DI} of
 317 7.5 and 8 having very similar performance profiles for event B1010 and B710 (Figure 9a-b) and TSR_{DI}
 318 slightly underperforming on average—but having a higher C_p at the end of the icing event (see Figure 8a
 319 and 8c)—the short energy payback time indicated for TSR_{DI} on Figure 10a-b should be neglected. During
 320 B510, the modified TSR strategies (TSR_{9DI} and $TSR_{9.5DI}$) provide higher energy yield and less ice-build up
 321 than operating at TSR_R resulting in a negative energy payback time.

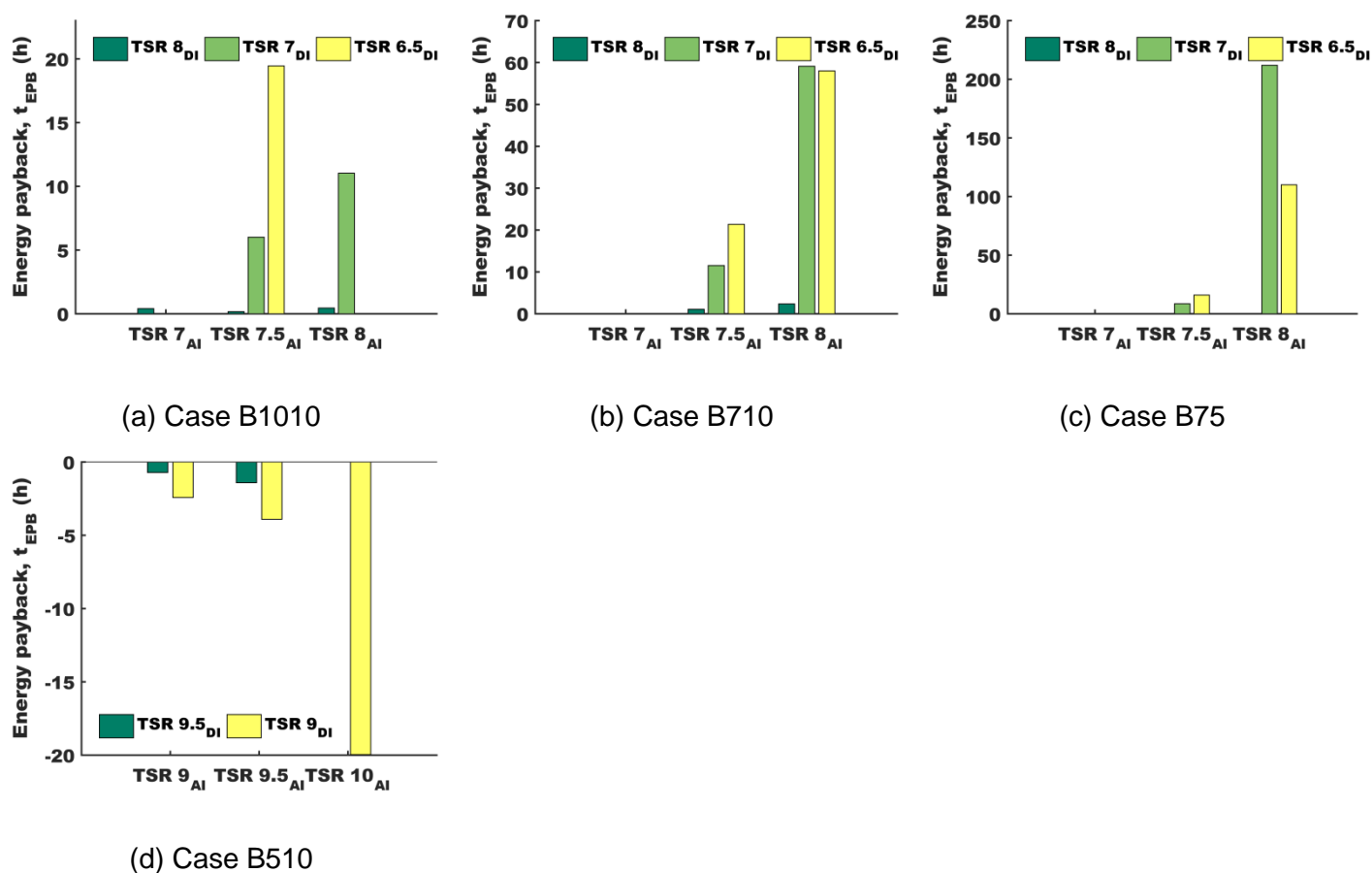


Figure 10a-d: Energy payback time for different tip-speed ratio after icing (TSR_{AI}) values for events B1010 (a), B710 (b), B75(c) and B510 (d).

322 3.1.3 Event C

323 Among Events A, B and C, Event C is characterised by having the lowest values for LWC and MVD and ice
 324 accretion rates. With Event C being simulated for a wind speed of 10 ms^{-1} and ambient temperatures of -5
 325 and -10°C , two cases are presented: C1010 and C105. Due to small ice build-up and shapes
 326 (approximately 0.15 to 0.4 kg for different TSR_{DI} values), the power losses are no greater than 1% over the

327
328

duration of the 4-hour icing events. In addition, the ice shapes are located on the pressure side of the leading edge of the blade (see Figure 11), leading to increased drag but minimal changes in lift [10].

329
330
331
332
333

From the energy payback time analysis, it can be concluded that the best option for operation for event C is to maintain operation at the reference TSR_R (i.e. 7.5). Energy payback time for all alternative operational strategies is relatively high for Event C, as there are minimal changes in C_p for different TSR_{DI} values (Figure 12a-b) and the ice deposition is low. For instance, by setting the TSR_{DI} to 7 and then operating at a TSR of 7.5 the energy recovery time would be either 24h (A105) or 14h (A1010) (see Figure 13a-b).

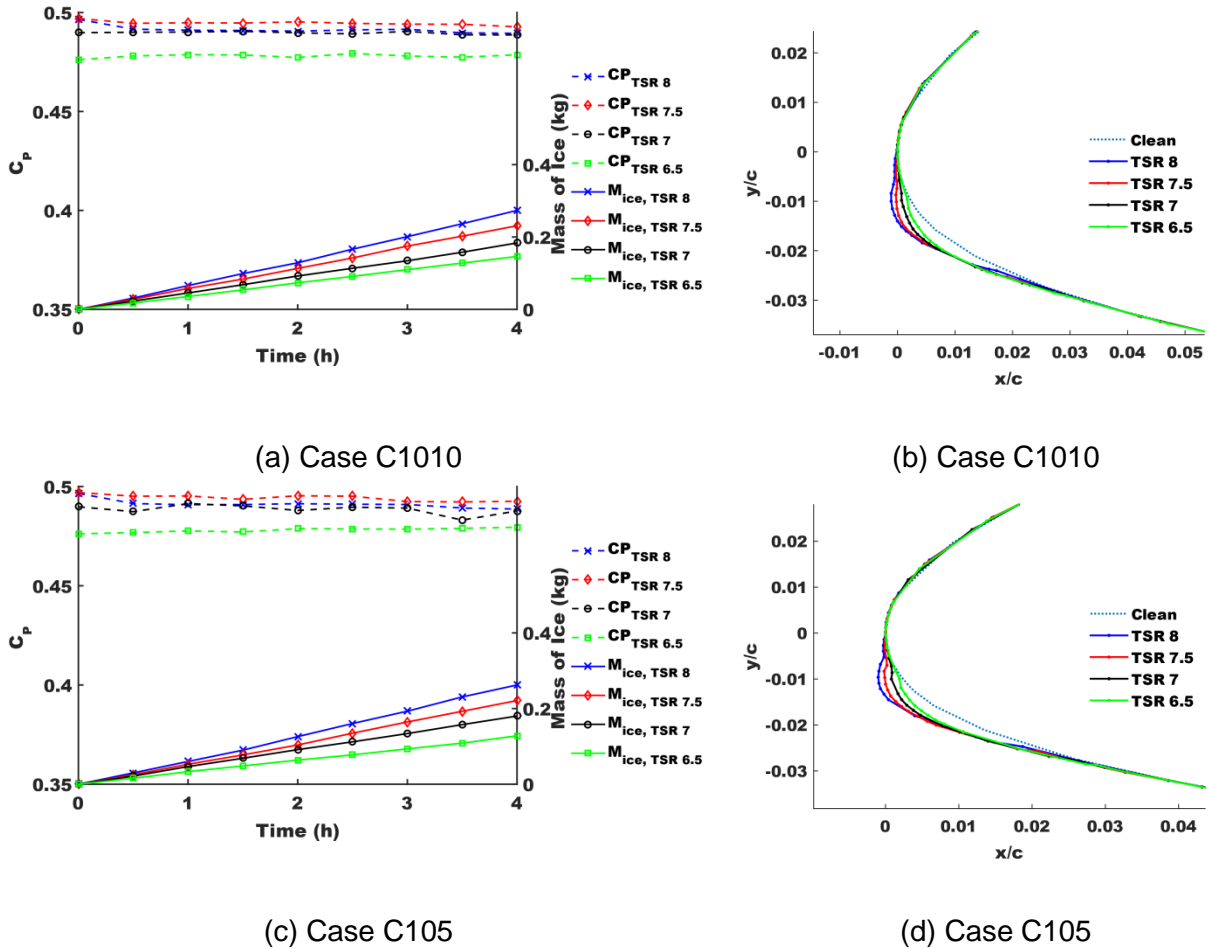
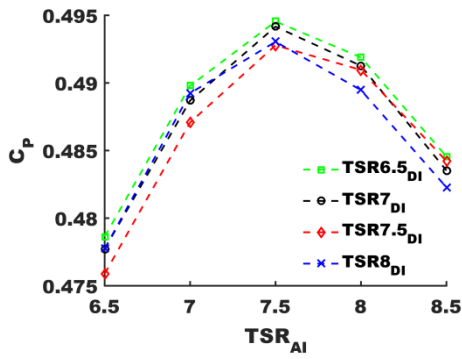
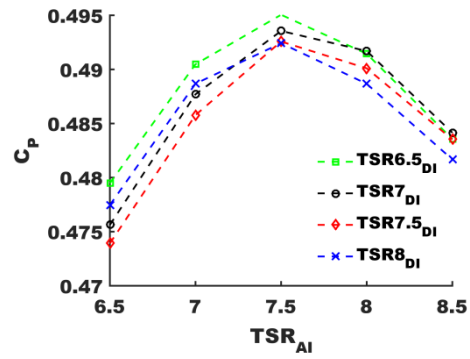


Figure 11a-d: Wind turbine C_p deterioration and ice accumulation per blade during events C1010 (a) and C105 (c) and ice shapes on section D at the end of events C1010 (b) and C710 (d).

334



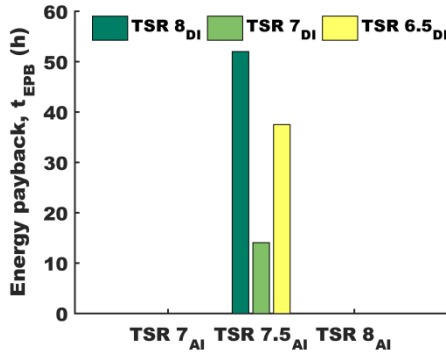
(a) Case C1010



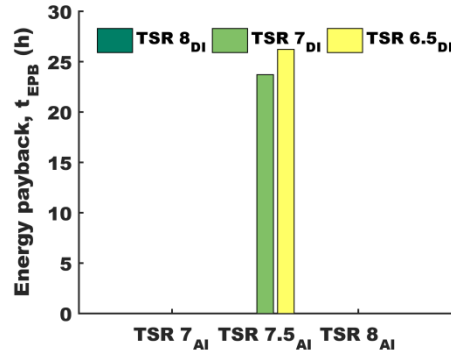
(b) Case C105

Figure 12a-b: Power characteristics of modified tip-speed ratio values after icing events C1010 (a) and C105 (b).

335



(a) Case C1010



(b) Case C105

Figure 13a-b: Energy payback time for different tip-speed ratio after icing (TSR_{Ai}) values for events C1010 (a) and C105 (b).

336

3.2 Further Work

337

338

339

340

341

342

343

As there are many different icing events that can last for a few hours to several days, the viability of the different operational strategies proposed in this study still needs further investigation. The current analysis utilised XFOIL, which enabled the aerodynamic performance of a large number of different ice shapes to be analysed with relatively low computational effort. However, the suggested ideal tip-speed ratio strategy for each event highly depends on the accuracy of the predicted aerodynamic penalties caused by ice build-up. In this study, the aerodynamic performance predictions are more reliable and accurate for the generated ice shapes without extreme irregularities and high curvature at the leading edge. Therefore, for the analysis

of icing events leading to more irregular shapes, higher fidelity tools, such as Navier-Stokes equation-based solvers, are required.

A predictive model based on XFOIL, or another tool that combines a panel method and integral boundary layer equations, could be developed to inform wind turbine controllers in real time, which would have significant benefits for wind farm operations. However, detection of ice accretion on wind turbines remains a challenge. This study has also highlighted some of the uncertainties and limitations of the panel method, so further work will be carried out to experimentally characterise and investigate them in more detail, so that improved predictive algorithms can be developed in the future.

The approach taken in this study of determining an energy payback time for different TSR operational strategies was found to be useful for both comparing the effectiveness of different strategies and indicating when normal operation can be maintained, or a different ice mitigation technique would be needed (e.g. an anti/de-icing system). Additional research will be carried out to evaluate the energy requirements to size and evaluate potential net energy gains/losses of using an anti-icing system in comparison to the alternative TSR strategies investigated for the events proposed in this study. Moreover, it will be interesting to consider how the model for predicting energy payback time can be modified to consider ice reduction mechanisms – such as melting, shedding and sublimation. If modelled, the ice mass would reduce after an icing event and the C_p would tend towards its clean blade value. However, this would be dependent on the weather conditions and the structural vibrations. In addition, the estimated energy payback times could be shorter if the ice deposition for an alternative operational strategy reduced faster than the ice accumulated for $TSR_{DI,R}$, but further investigations are required to accurately model this. The model could also be extended to determine which strategy is the most effective when vibration and structural analysis is incorporated. The viability of a TSR strategy would depend on the wind turbine type, local weather parameters and structural damage limitations. As rotational speed would actually decrease on variable-speed and variable-pitch wind turbines due to ice formation, a further improvement to the model could be achieved by modelling the transient behaviour of the TSR during ice build-up. This will be particularly beneficial when analysing long severe icing events.

4 Conclusion

This paper examined the effectiveness of rotational speed modifications for the NREL 5 MW reference wind turbine during icing conditions. The turbine was simulated for three icing events, three wind speeds and two ambient temperatures, resulting in 12 different cases. To compare the effectiveness of each strategy, an energy payback time parameter was modelled to determine when slowing a wind turbine down during an

376 icing event would provide overall more energy than a conventional strategy. The obtained results
377 suggested that alternative strategies for mitigating ice losses, realised by tip-speed ratio modifications, are
378 most effective for short and severe icing events. For LWC of $5 \times 10^{-4} \text{ kg.m}^{-3}$ and MVD of $25 \times 10^{-6} \text{ m}$, the
379 energy that is lost due to reducing the tip-speed ratio can be recovered within 0.5-2.5 hours post-icing
380 event, thereby reducing the power losses from 7% to 23% and ice mass accreted on each blade from 20%
381 to 30%. However, for longer and milder events, the energy recovery time is significantly longer (around 10-
382 28h) suggesting the reference design strategy should be maintained. Additionally, the possibility for
383 applying the TSR modification strategies should be considered carefully, as only limited ice mass would be
384 acceptable due to structural constraints. Furthermore, the need for higher fidelity analysis tools is apparent
385 for longer icing events, with XFoil being more effective for modelling short rime and glaze icing conditions,
386 which do not result in severe horn-like shapes. Where previous wind turbine icing studies have tended to
387 focus on just ice-induced power losses, this study has demonstrated the importance of considering a wind
388 turbine blade's power characteristics and energy production throughout an icing event and performance
389 once an icing event ends. The energy payback time method presented can identify which tip-speed ratio
390 modifications can be used during and after an icing event, provided local meteorological conditions can be
391 accurately predicted. Thus, this work will be of significant interest to wind turbine operators working in cold
392 climate locations.

393

394 **Figures and table**

395 Figure 1: Discretised NREL 5 MW blade and the selected 2D sections for ice accretion analysis.

396 Figure 2a-b: NREL 5 MW reference wind turbine TSR operational limits defined by the limiting rotational
397 speeds of the electrical generator (a) and how the power coefficient varies at different TSR (b).

398 Figure 3a-b: Power output (a) and cumulative energy (b) during and after an icing event for a wind turbine
399 operating with a reference (TSR_R) or modified (TSR_M) tip-speed ratio strategy.

400 Figure 4a-f: Wind turbine power coefficient degradation and total ice mass accumulation on a single blade
401 during events A1010 (a), A105 (b), A710 (c), A75 (d), A510 (e) and A55 (f).

402 Figure 5a-f: Ice shapes on Section D for event cases A1010 (a), A105 (b), A710 (c), A75(d), A510 (e) and
403 A55 (f).

404 Figure 6a-f: Power characteristics of modified tip-speed ratio values after icing events A1010 (a), A105 (b),
405 A710 (c), A75(d), A510 (e) and A55 (f).

406 Figure 7a-f: Energy payback time for different tip-speed ratio after icing (TSR_{AI}) values for events A1010
407 (a), A105 (b), A710 (c), A75(d), A510 (e) and A55 (f).

408 Figure 8a-h: C_p deterioration and ice accumulation during events B1010 (a), B710 (c), B75 (e), B510 (g) and
409 ice shapes on section D at the end of events B1010 (b), B710 (d), B75 (f), B510 (h).

410 Figure 9a-d: Power characteristics of modified tip-speed ratio values after icing events B1010 (a), B710 (b),
411 B75(c), B510 (d) and B55 (e).
412 Figure 10a-d: Energy payback time for different tip-speed ratio after icing (TSR_{AI}) values for events B1010
413 (a), B710 (b), B75(c) and B510 (d).
414 Figure 11a-d: C_p deterioration and ice accumulation during events C1010 (a) and C105 (c) and ice shapes
415 on section D at the end of events C1010 (b) and C710 (d).
416 Figure 12a-b: Power characteristics of modified tip-speed ratio values after icing events C1010 (a) and
417 C105 (b).
418 Figure 13a-b: Energy payback time for different tip-speed ratio after icing (TSR_{AI}) values for events C1010
419 (a) and C105 (b).
420
421 Table 1: Definition of icing events A, B and C, at different wind speeds (V) and temperature (T).
422

423 References

- 424 [1] Anon, Global Wind Report, GWEC. (2018) 16-60.
- 425 [2] V Lehtomaki, Emerging from the cold, Wind Power. 2019 (2016) 1-
426 <https://www.windpowermonthly.com/article/1403504/emerging-cold>.
- 427 [3] G Fortin, J Perron, A Ilinca, Behaviour and Modeling of Cup Anemometers under Icing Conditions,
428 IWAIS. 11 (2005) Montreal.
- 429 [4] A Krenn, PJ Jordaens, M Wadham-Gagnon, N Davis, N Clausen, V Lehtomaki, et al., Wind Energy in
430 Cold Climates Available Technologies - report, (2016).
- 431 [5] RE Bredesen, R Cattin, N Clausen, N Davis, PJ Jordaens, Z Khadri-Yazami, et al., Wind Energy
432 Projects in Cold Climates, (2017).
- 433 [6] V Turkia, S Huttunen, T Wallenius, Method for estimating wind turbine production losses due to icing,
434 (2013).
- 435 [7] O Parent, A Ilinca. Anti-icing and de-icing techniques for wind turbines: Critical review, Cold Regions
436 Science and Technologies. 65 (2011) 88-96.
- 437 [8] N Dalili, A Edrisy, R Carriveau. A Review of Surface Engineering Issues Critical to Wind Turbine
438 Performance, Renewable & Sustainable Energy Reviews. 13 (2007) 428-438.
- 439 [9] L Battisti, Chapter 4 Icing Process, Wind Turbines in Cold Climates, Springer, Switzerland, 2015, pp.
440 177-248.
- 441 [10] M Bragg B., A Broeren P., L Blumenthal A. Iced-airfoil aerodynamics, Progress in Aerospace Sciences.
442 (2005) 323-362.

-
- 443 [11] B Tammelin, M Cavaliere, H Holttinen, C Morgan, H Seifret, K Santti, Wind Energy Production in Cold
444 Climates (WECCO), (2000).
- 445 [12] T Laakso, I Baring-Gould, M Durstewitz, R Horbaty, A Lacroix, E Peltola, et al., State-of-the-art of wind
446 energy in cold climates, (2010).
- 447 [13] B Tammelin, H Seifret, Large Turbines Go into Cold Climate Regions, EWEC 2001. Copenhagen
448 (2001).
- 449 [14] M Etemaddar, M Hansen, T Mo. Wind turbine aerodynamic response under atmospheric icing
450 conditions, Wind Energy. 17 (2012) 241-265.
- 451 [15] N Davis, AN Hahmann, N Clausen, M Zagar, Icing Impacts on Wind Energy Production, DTU. (2014).
- 452 [16] L Hu, X Zhu, C Hu, J Chen, Z Du. Wind turbine ice distribution and load response under icing
453 condition, Renewable Energy. 113 (2017) 608-619.
- 454 [17] R Cattin, Icing of Wind Turbines, Eلفorsk. 12:13 (2012) 23.
- 455 [18] M Homola, M Virk, M Nicklasson, P J. Performance losses due to ice accretion for a 5 MW wind
456 turbine, Wind Energy. 15 (2012) 379-389.
- 457 [19] A Zanon, M Gennaro De, H Kuhnelt. Wind energy harnessing of the NREL 5 MW reference wind
458 turbine in icing conditions under different operational strategies, Renewable Energy. 115 (2018) 760-772.
- 459 [20] D Brillembourg, Turbines Under Atmospheric Icing Conditions - Ice Accretion Modelling,
460 Aerodynamics, and Control Strategies for Mitigating Performance Degradation, Wind Energy. 20 (2013)
461 601-617.
- 462 [21] W Wright, User's Manual for LEWICE Version 3.2, (2008).
- 463 [22] W Wright B., Validation Results for LEWICE 3.0, (2005).
- 464 [23] D Marten, J Wendler, Qblade Guidelines, (2013).
- 465 [24] M Drela, XFOIL: An Analysis and Design System for Low Reynolds Number Airfoils, Low Reynolds
466 Number Aerodynamics. (1989).
- 467 [25] J Jonkman, S Butterfield, W Musial, G Scott, Definition of a 5-MW Reference Wind Turbine of Offshore
468 System Development, (2009).
- 469 [26] G Poots, Ice and Snow Accretion on Structures, 1st ed., Research Studies Press, Exeter, 1996.
- 470 [27] MC Pederson, H Sorenson, N Swytink-Binnema, B Martinez, T Condra. Measurements from a cold
471 climate site in Canada: Boundary conditions and verification methods for CFD icing models for wind
472 turbines, Cold Regions Science and Technologies. 147 (2018) 11-21.
- 473 [28] S Cober G., G Isaac A., J Strapp W. Aircraft Icing Measurement in East Coast Winter Storms, Journal
474 of Applied Meteorology. 34 (1994) 88.

-
- 475 [29] F Lamraoui, G Fortin, R Benoit, J Perron, C Masson. Atmospheric icing impact on wind turbine
476 production, *Cold Regions Science and Technologies*. 100 (2014) 36-49.
- 477 [30] W Lewis, A Flight Investigation of the Meteorological Conditions Conducive to the Formation of Ice on
478 Airplanes, *National Advisory Committee for Aeronautics*. 1393 (1947) 25.
- 479 [31] L Chen, B Tan, G Kvamsto Nils, M Johannessen Ola. Winter cyclone/anticyclone activity over China
480 and its relation to upper tropospheric jets, *Tellus AL Dynamic Meteorology and Oceanology*. 66 (2014).
- 481